

# High-Accuracy Optical Fiber Transfer Delay Measurement using Fiber-Optic Microwave Interferometry

Shupeng Li, Ting Qing, Jianbin Fu, Xiangchuan Wang, and Shilong Pan, *Senior Member, IEEE*

**Abstract**—Optical fiber transfer delay (OFTD) measurement with high accuracy and stability is an urgent demand for many applications such as fiber-optic sensors and fiber-based distributed systems. In this article, we propose a novel method using fiber-optic microwave interferometry to meet the above practice demand. Two incoherent optical carriers with different wavelengths are coupled into an intensity modulator driven by a microwave signal. The intensity-modulated signal is then divided into two portions through a dense wavelength division multiplexer. One portion directly passes through the reference path while the other undergoes the transfer delay of a fiber under test (FUT). After photo-detection, two probe signals that undergo different delays are recovered and superimposed. By sweeping the microwave frequency, periodic microwave interference fringe is generated. Then, OFTD measurement is achieved by measuring the frequency of the last valley in the interference fringe. Experimental results show that a system stability of  $\pm 0.02$  ps, an accuracy of  $\pm 0.07$  ps, and a measurement range of at least 500 m are achieved.

**Index Terms**—Optical transfer delay measurement, fiber-optic microwave interferometry, microwave measurement.

## I. INTRODUCTION

OPTICAL fiber transfer delay (OFTD) measurement with high accuracy is critical for applications in fiber-optic sensors, optical phased array antenna systems, and optical fiber communications [1]-[11]. In recent decades, a variety of technologies have been proposed for the OFTD measurement, such as time domain measurement techniques, frequency domain measurement techniques, and the measurement techniques based on phase-derived ranging [12].

For the time domain based techniques, a widely used method is pulse-based optical time domain reflectometry (OTDR) [13],

This work was supported in part by the National Natural Science Foundation of China (Nos. 62075095 and 61527820), Young Elite Scientists Sponsorship Program by CAST (2018QNR001), and Fundamental Research Funds for the Central Universities. (Corresponding authors: Xiangchuan Wang and Shilong Pan)

Shupeng Li, Ting Qing, Xiangchuan Wang and Shilong Pan are with the Key Laboratory of Radar Imaging and Microwave Photonics, Ministry of Education, Nanjing University of Aeronautics and Astronautics, Nanjing, 210016, China. (Email: wangxch@nuaa.edu.cn, pans@nuaa.edu.cn).

Jianbin Fu is with the Key Laboratory of Radar Imaging and Microwave Photonics, Ministry of Education, Nanjing University of Aeronautics and Astronautics, Nanjing, 210016, China, and also with the Suzhou LiuYaoSi Information Technologies Co., Ltd, Suzhou, 215500, China.

which features large measurement range (typically 2 ms). However, due to the employment of a relatively wide probe pulse, this method has a low accuracy (typically 10 ns at 1 km). To improve the accuracy, a correlation OTDR with pseudorandom pulse sequences or chaotic waveform was proposed by correlating the reference and echo probe signals to achieve OFTD measurement [14], [15]. The typical accuracy was improved to 0.3 ns at 20 km. However, the correlation OTDR depends on high-speed analog to digital converter (ADC), inducing a huge amount of computation.

For the frequency domain based techniques, optical frequency domain reflectometry (OFDR) is the most mature commercial technology, which usually applies linearly frequency swept light generated from a tunable laser [16]. The beat of reference and echo probe light is used for the OFTD measurement. Benefitting from the wide frequency range of the probe light, OFDR features high accuracy in short-distance measurement. However, its accuracy will be significantly degraded with the increase of fiber length due to the frequency noise of the tunable laser (typically 5 ps at 2 km). Besides, limited by the coherence length of the tunable laser, OFDR usually has a small measurement range (typically several kilometers). To improve the measurement range, a mode-locking method was proposed by converting the OFTD measurement into the repetition frequency measurement of the mode-locked pulse [17] with a typical accuracy of 250 ps at 100 km. However, the implementation of long-term stable mode-locking is very complicated and time-consuming. To avoid the complex mode-locking operation and reduce the measurement time, a simpler technique based on a free-running laser configuration was proposed. The mode beating frequency was measured to determine the OFTD with the measurement time reduced to several minutes [18]. To further enhance the measurement speed, J. W. Dong *et al.* proposed a phase-locked-loop-based method [19] featuring a higher speed of several seconds per measurement and a better accuracy of  $\pm 1$  ps at 50 km. The key to this method is converting the OFTD measurement into the frequency measurement of a RF signal. Nevertheless, a 5-km fiber should be inserted in advance to eliminate the dead zone, which introduces a measurement uncertainty of 0.5 ps.

The OFTD measurement based on phase-derived ranging is a newly proposed technology. For example, reference [20] converts the OFTD measurement into the phase variation

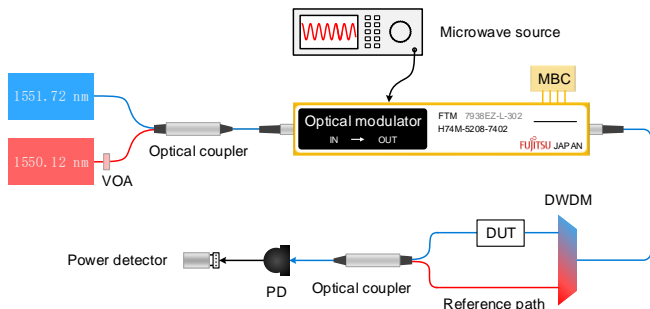


Fig. 1. Experimental set-up for the fiber-optic microwave interferometer. VOA: variable optical attenuator; MBC: modulator bias controller; DWDM: dense wavelength division multiplexer; DUT: device under test; PD: photodetector.

measurement of a RF signal, in which the  $2\pi$  phase ambiguity is solved by linear microwave frequency sweeping. This method has a high accuracy of  $\pm 0.1$  ps and a large dynamic range of 20 km. However, when measuring large OFTD (e.g., long fiber), linear frequency sweeping requires thousands of frequency points, which would greatly increase the measurement time (typically several seconds). To improve the measurement speed, a nonlinear frequency sweeping method with a novel phase unwrapping algorithm is proposed to resolve the  $2\pi$  phase ambiguity [21]. However, due to the lack of a reference path to eliminate system variation, this method has a relatively low system stability (typically  $\pm 0.04$  ps).

The key performance of above-mentioned OFTD measurement approaches is summarized in Table I, in which the system stability, measurement accuracy and measurement range are considered.

In this paper, an OFTD measurement based on fiber-optic microwave interferometry featuring high accuracy, high stability, and simple structure is characterized. A microwave modulated signal is divided into two portions and transmitted through an optical reference path and measurement path, respectively. After photo-detection, microwave interference occurs. As the microwave frequency is scanned, an interference fringe is generated to derive the OFTD. Similar concepts can also be seen in the community of fiber sensing and Lidar system [22-23]. Firstly, the principle and system structure is given in section II. Then experimental demonstration and discussion are introduced in section III. In an experiment, an ultrahigh-accuracy variable optical delay line and a 500-m fiber are used as the devices under test (DUTs), validating that a system stability of  $\pm 0.02$  ps, an accuracy of  $\pm 0.07$  ps, and a measurement range of at least 500 m can be achieved. And finally, the conclusion is drawn in section IV.

## II. PRINCIPLE

The schematic diagram of the proposed OFTD measurement method based on fiber-optic microwave interferometry is shown in Fig.1. Two incoherent optical carriers are generated by a 1550.12-nm laser source and a 1551.72-nm laser source. A variable optical attenuator (VOA) is used to finely tune the optical power of the 1550.12-nm carrier. Then, the two carriers are coupled into an intensity modulator driven by a swept

TABLE I  
PERFORMANCE OF OFTD MEASUREMENT METHODS

Methods	Stability	Accuracy	Range
OTDR [13]	~	10 ns	1 km
C-OTDR [14]	~	0.3 ns	20 km
OFDR [16]	~	5 ps	2 km
Fiber laser [17]	~	250 ps	100 km
Fiber laser [18]	~	$\pm 28$ ps	100 km
Phase-locked loop [19]	$\pm 0.538$ ps	$\pm 1$ ps	50 km
Phase-derived ranging [20]	$\pm 0.1$ ps	$\pm 0.1$ ps	20 km
Phase-derived ranging [21]	$\pm 0.04$ ps	$\pm 0.05$ ps	37 km

microwave signal. The intensity modulated signal is divided into two portions through a dense wavelength division multiplexer (DWDM). One portion goes directly through the reference path while the other is transmitted through a DUT in the measurement path. After photo-detection, two microwave signals with different delays are recovered and superimposed. As the frequency of the microwave signal is linearly scanned, a periodic interference fringe is generated to calculate the OFTD.

Mathematically, the optical field of the intensity modulated signal launched into the DWDM can be written as

$$E_M(t) = E_p(1 + M \cos \omega_m t) \exp(j\omega_p t) + E_r(1 + M \cos \omega_m t) \exp(j\omega_r t) \quad (1)$$

where  $M$  is the index of modulation,  $\omega_m$  is the angular frequency of the microwave signal,  $E_r$  and  $E_p$  are the amplitudes,  $\omega_r$  and  $\omega_p$  are the angular frequencies of the optical carriers, respectively. Then, the input signal of the PD can be described as

$$E(t) = \frac{\alpha E_p}{\sqrt{2}} [1 + M \cos \omega_m (t - \tau_0 - \tau)] \exp[j\omega_p (t - \tau_0 - \tau)] + \frac{E_r}{\sqrt{2}} (1 + M \cos \omega_m t) \exp(j\omega_r t) \quad (2)$$

where  $\tau_0$  is the delay difference between the measurement path and the reference path without DUT,  $\alpha$  and  $\tau$  are the loss and transfer delay of DUT, respectively. After square-law detection in the PD, the recovered microwave signal with the frequency of  $\omega_m$  is

$$i(t) = \eta \alpha^2 E_p^2 M \cos \omega_m (t - \tau_0 - \tau) + \eta E_r^2 M \cos \omega_m t \quad (3)$$

where  $\eta$  is the responsivity of the PD. After simplification, the log amplitude of  $i(t)$  can be given by

$$A(\omega_m) = 10 \log_{10} (E_r^4 + \alpha^4 E_p^4 + 2\alpha^2 E_p^2 E_r^2 \cos \omega_m (\tau_0 + \tau)) + 20 \log_{10} (\eta M) \quad (4)$$

It can be seen that, as the microwave frequency is scanned, the

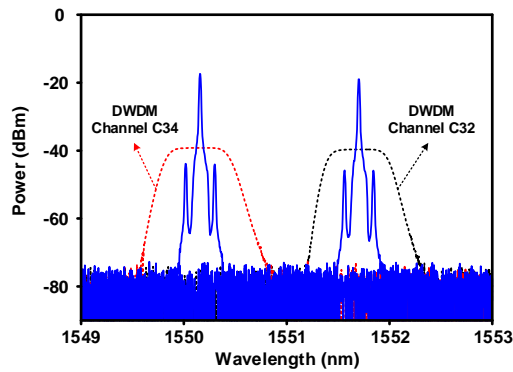


Fig. 2. Optical spectrum of the generated dual-wavelength intensity modulated signal when a 10 GHz RF signal is applied. The red and black dotted lines are the spectral responses of the DWDM channel C34 and C32, respectively.

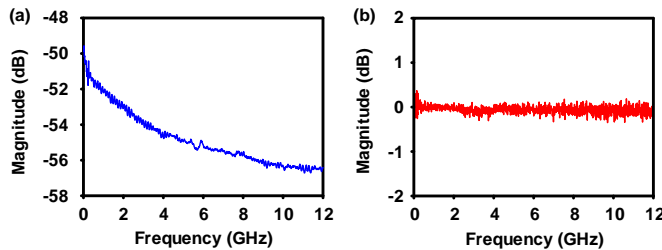


Fig. 3. Frequency response of the measurement system. (a) before calibration; (b) after calibration.

log amplitude  $A(\omega_m)$  varies with frequency and has a period of  $1/(\tau_0 + \tau)$ . Thus, the frequency location of each valley in the microwave interference fringe can be expressed as

$$f_k = \left(k - \frac{1}{2}\right) \cdot \frac{1}{\tau_0 + \tau} \quad (5)$$

where  $k$  is the ordinal number of the valley. Then, the transfer delay of the DUT can be given by

$$\tau = \left(k - \frac{1}{2}\right) \cdot \frac{1}{f_k} - \tau_0 \quad (6)$$

It should be noted that, before measuring the DUT, an initial measurement should be performed to achieve  $\tau_0$ , wherein the two test ports are directly connected. In addition, the theoretical delay resolution can be derived from (6) and written as

$$\tau_{\text{res}} = \left(k - \frac{1}{2}\right) \cdot \frac{f_{\text{res}}}{f_k^2} = (\tau + \tau_0) \cdot \frac{f_{\text{res}}}{f_k} \quad (7)$$

where  $f_{\text{res}}$  is frequency step of the microwave swept signal. As seen from (7), the theoretical delay resolution is inversely proportional to  $f_k$ . Therefore, to acquire a higher delay resolution, the last valley with the largest frequency in the measured interference fringe should be used to calculate the OFTD.

### III. EXPERIMENT AND DISCUSSION

An experiment is performed based on the setup shown in Fig.

1. A 4-port tunable laser system source (TLS, Keysight N7714A) with a linewidth of  $< 100$  kHz generates two optical carriers, wherein the carrier wavelength is set to 1550.12 nm (center wavelength of DWDM ITU channel C34) and 1551.72 nm (center wavelength of DWDM ITU channel C32), respectively. The power of the 1550.12-nm carrier is finely tuned by a variable optical attenuator (VOA, Keysight N7764A) with a resolution of 0.01 dB. Then, the two carriers are coupled into a Mach-Zehnder modulator (MZM, Fujitsu FTM7928FB) driven by a microwave signal from a microwave vector network analyzer (VNA, R&S ZVA67). A modulator bias controller (MBC, YY Labs Inc.) is used to keep the MZM biased at the quadrature point. The intensity modulated signal is then divided by a dense wavelength division multiplexer (DWDM). A photodetector (PD, Discovery DSC40S) with a 3-dB bandwidth of 14 GHz and the VNA are used to extract the magnitude. It is worth mentioning that using a single PD to detect two optically carried RF signals can help to reduce system complexity and improve stability. An optical spectrum analyzer (OSA, Yokogawa AQ6370C) monitors the optical signals with a resolution of 0.02 nm. To stabilize the measurement system, an incubator with a precision of  $\pm 0.1$  °C is used to control the temperature of DWDM, reference path, and optical coupler.

Figure 2 shows the optical spectrum of the dual-wavelength intensity-modulated signal when a 10 GHz RF signal is applied. It can be seen that the two carriers are located exactly at the centers of the DWDM channel C32 and C34, respectively. The  $\pm 1$ -st-order sidebands are in the flat-top region of the DWDM, which ensures  $\pm 1$ -st-order sidebands immune to the suppression. Figure 3 shows the frequency response of the proposed measurement system before calibration and after calibration, wherein the measurement path is disconnected. As can be seen from Fig. 3(a), the wideband frequency response of the modulator and PD is curved, inducing a worse effect on searching for the frequency location of the valley in the interference fringe. Therefore, a thorough calibration should be used to obtain a flat system response. As shown in Fig. 3(b), the normalized system response is flat and its fluctuation is less than  $\pm 0.5$  dB.

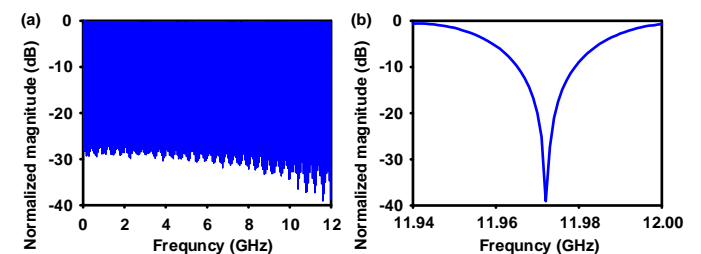


Fig. 4. (a) The measured microwave interference fringe without DUT. (b) The last valley of the measured microwave interference fringe.

#### A. Stability

To assess the system stability, the measurement of  $\tau_0$  without DUT is performed by directly connecting two test ports of the measurement path.

Figure 4 shows the measured microwave interference fringe

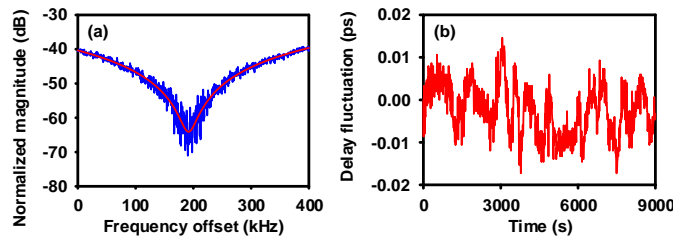


Fig. 5. Evaluation of system stability. (a) The measured microwave interference fringe with a frequency step of 500 Hz, wherein the start frequency is 11.97141 GHz and the red line is the fitted line. (b) The fluctuation of  $\tau_0$ .

with a repetition period of  $\sim 63.12$  MHz. According to (5), the frequency location of the first valley is  $\sim 31.56$  MHz =  $(1-1/2) \times 63.12$  MHz, which is larger than the minimum measurable frequency point (10 MHz) of the VNA. Therefore, the first valley is included in the measured interference fringe ensuring that the ordinal number of the last valley can be determined as 191 without ambiguity. According to (7), as the frequency location of the last valley is  $\sim 11.972$  GHz, a delay resolution of 1 fs requires a frequency step of at least 752.3821 Hz. Thus, a fine frequency sweeping with a frequency step of 500 Hz around 11.972 GHz is applied. The measured microwave interference fringe is shown in Fig. 5(a), wherein the magnitude fluctuation at the valley is  $\sim 10$  dB. In peak seeking, the 10-dB magnitude fluctuation will cause a large measurement uncertainty. So, we fit the interference fringe to extract the frequency of the last valley (11.9716015 GHz). Finally,  $\tau_0$  can be calculated as 15.912658 ns =  $(191-1/2)/11.9716015$  GHz. To assess the long-term system stability, the measurement of  $\tau_0$  is performed for 9000 seconds. As can be seen in Fig. 5(b), the fluctuation of  $\tau_0$  is within  $\pm 0.02$  ps, which shows high stability. In addition, it needs to be explained that, because the resolution bandwidth (RBW) of the VNA is increased from 1 kHz to 100 Hz, the valley magnitude shown in Fig. 5(a) is about 25 dB lower than that shown in Fig. 4(b).

According to (6), the delay uncertainty can be given by

$$\delta\tau = \left(k - \frac{1}{2}\right) \frac{\delta f}{f_k^2} + \delta\tau_0 = (\tau + \tau_0) \frac{\delta f}{f_k} + \delta\tau_0 \quad (8)$$

where  $\delta f$  is the uncertainty of the frequency location,  $\delta\tau_0$  is determined by the temperature fluctuation  $\delta T$  and the DWDM thermal coefficient  $\delta n$  (11 ppm). In our experiment,  $\delta T$  is determined by the temperature control precision (0.1 °C) of the incubator. Therefore, the theoretical value of  $\delta\tau_0$  is calculated as 0.0174 ps =  $\tau_0 \delta T \delta n$ . In addition, as seen in Fig. 6,  $\delta f$  is also determined by the amplitude uncertainty  $\delta A$ , interference depth  $D$ , and free spectral range  $FSR = 1/(\tau + \tau_0)$ . According to (4), these parameters satisfy the following equations:

$$\begin{cases} 20 \log_{10} \left( A \left( \frac{FSR}{2} + \delta f \right) \right) - 20 \log_{10} \left( A \left( \frac{FSR}{2} \right) \right) = \delta A \\ 20 \log_{10} (A(FSR)) - 20 \log_{10} \left( A \left( \frac{FSR}{2} \right) \right) = D \end{cases} \quad (9)$$

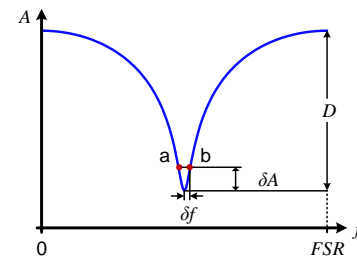


Fig. 6. The simulated interference fringe.

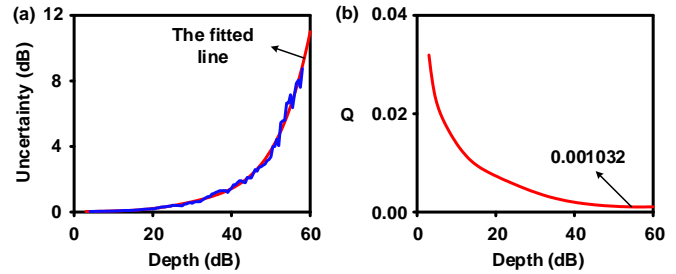


Fig. 7. The amplitude uncertainty (a) and  $Q$  value (b).

After simplification, (9) can be rewritten as

$$Q = \frac{\delta f}{FSR} = \frac{1}{2} - \frac{1}{2\pi} \arccos \left( 2 \times \frac{10^{\delta A/10} - 1}{10^{D/10} - 1} - 1 \right) \quad (10)$$

Then, (8) can be rewritten as

$$\delta\tau = \frac{Q}{f_k} + \delta\tau_0 \quad (11)$$

By changing the attenuation of the VOA, different interference depths are achieved while the corresponding amplitude uncertainty is also obtained as shown in Fig. 7(a), wherein the RBW of the VNA is set to 100 Hz. Then, according to (10),  $Q$  can be simulated. It can be seen from Fig. 7(b) that  $Q$  decreases monotonically as the interference depth increases and eventually tends to 0.001032. In our experiment, limited by the 3-dB bandwidth of the PD and linear phase bandwidth of the DWDM,  $f_k$  is  $\leq 12$  GHz. Therefore, the theoretical delay uncertainty induced by the frequency measurement is  $\geq 0.086$  ps. To reduce the measurement uncertainty, fitting is applied in our experiment. Experimental results show that the total delay uncertainty can be reduced to 0.02 ps.

### B. Accuracy

To verify the measurement accuracy, a motorized variable optical delay line (MDL, General Photonics MDL-002) with a resolution of  $< 1$  fs and an accuracy of  $\pm 0.01$  ps is used as the ultrahigh-accuracy reference.

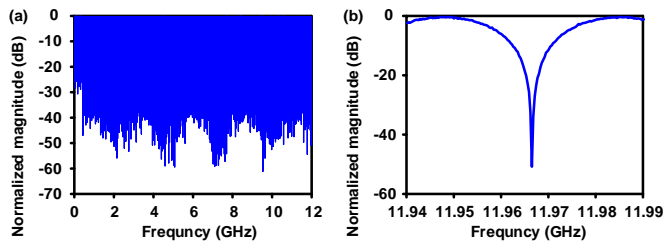


Fig. 8. (a) The measured microwave interference fringe under the test of MDL when it is at the zero position. (b) The last valley of the measured microwave interference fringe.

Figure 8 shows the interference fringe when the MDL was connected to the measurement path and set at the zero position. It can be seen that the ordinal number of the last valley is 320 and the frequency location is  $\sim 11.9665$  GHz. According to (5), as the OFTD changes, the location variation of a valley can be given by

$$\Delta f_k = -\frac{f_k^2}{k-1/2} \Delta \tau \quad (12)$$

where the negative sign indicates the direction of the OFTD variation. According to (12), if the MDL delay changes from 0 to 10 ps, the frequency location shift of the last valley is about  $-4.482$  MHz. Therefore, we sweep the frequency from 11.9615 GHz to 11.967 GHz with a step of 1 kHz and then change the MDL delay from 0 ps to 10 ps with a step of 1 ps. The measured interference fringes are shown in Fig. 9. Due to the MDL insertion loss variation of  $\pm 0.5$  dB, the depths of the 11 interference fringes are different. To verify the reliability of the experiment, three measurements were applied and the corresponding derived OFTDs are shown in Fig. 10(a), which agree well with the set values. As can be seen from Fig. 10(b), the OFTD deviation from the set value is within  $\pm 0.07$  ps. Thus, an accuracy of  $\pm 0.07$  ps is achieved.

### C. Measurement Range

From (5), it can be seen that the ordinal number  $k$  achieved by counting the number of interference fringe valleys has an integer ambiguity, when the frequency location of the first valley  $f_1$  is less than the minimum frequency of the microwave swept signal  $f_{\min}$ . Therefore, the maximum measurable delay can be calculated as  $1/2f_{\min} - \tau_0$ . In the experiment,  $f_{\min}$  is determined by the VNA with a minimum output frequency of 10 MHz. Thus, the theoretically maximum measurable delay is 34.144314 ns.

To improve the measurement range, the integer ambiguity of the ordinal number is resolved by linear frequency sweeping and fast Fourier transform (FFT). First, a microwave interference fringe in the frequency range of  $[f_s, f_e]$  is measured. Then, a coarse  $FSR$  can be calculated as  $f_i$  by FFT. Finally, the number of valleys included in the frequency range of  $(0, f_s)$  can be derived as  $N = \text{floor}(f_s/f_i + 1/2)$ , where  $\text{floor}(\cdot)$  denotes round towards minus infinity. According to Nyquist sampling law, the maximum measurable delay is determined by the frequency sweep step. In the experiment, the maximum number of measurement points is 60001 (limited by VNA) and the

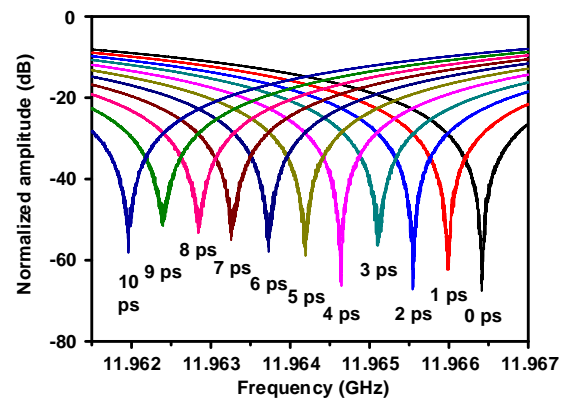


Fig. 9. The measured microwave interference fringes under the test of MDL when its delay changes from 0 ps to 10 ps with a step of 1 ps.

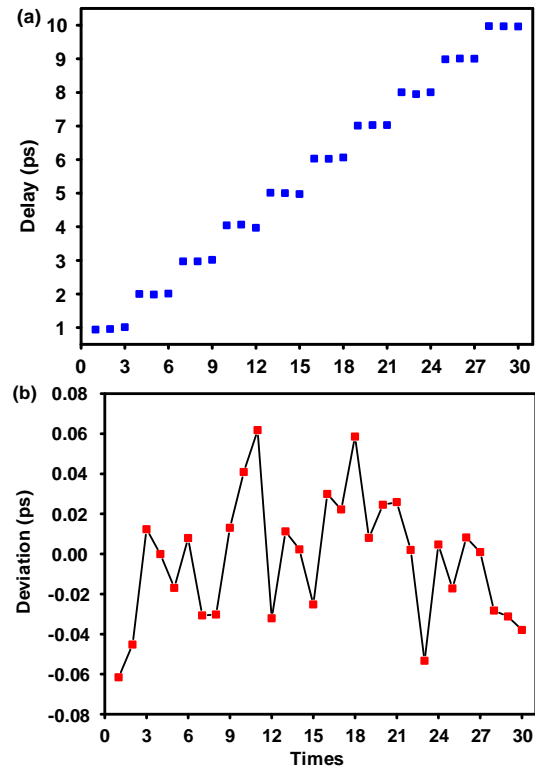


Fig. 10. Evaluation of measurement accuracy. (a) The measured MDL delay when it changes with a step of 1 ps. (b) The measurement deviation.

frequency range is [10 MHz, 12 GHz]. Therefore, in a single scan, the frequency step  $f_{\text{res}}$  can reach  $199.833 \text{ kHz} = (12 \text{ GHz} - 10 \text{ MHz}) / 60000$ . The maximum measurable delay is calculated as  $\sim 2.486 \text{ us} = 1/2f_{\text{res}} - \tau_0$ . If the VNA's memory capacity is increased, the number of measurement points can be significantly increased. Then, the measurement range can be greatly improved. In addition, inspired by signal processing techniques coming from FMCW radars, the measurement range can also be improved using a wideband LFM signal instead of the current stepped frequency signal.

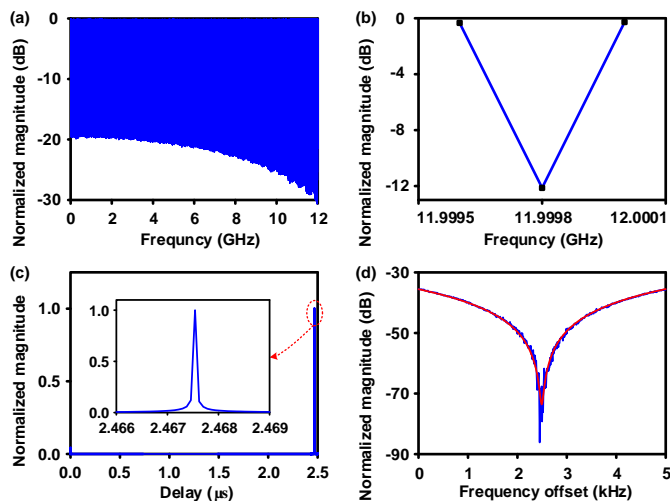


Fig. 11. Evaluation of measurement range. (a) The measured microwave interference fringe under the test of a 500-m fiber. (b) The last valley of the measured microwave interference fringe. (c) The fast Fourier transform of the measured interference fringe with linear magnitude. (d) The measured interference fringe with a frequency step of 100 Hz and an RBW of 10 Hz, wherein the start frequency is 11.9998225 GHz and the red line is the fitted line.

To demonstrate the measurement range in a single scan, a 500-m fiber is measured. Figure 11(a) shows the measured interference fringe. After the logarithmic amplitude is converted into linear amplitude, Fig. 11(c) is achieved by FFT. Then, the coarse  $FSR$  is calculated as  $405.2592 \text{ kHz} = 1/(2467.556296 \text{ ns})$ . Thus, the ordinal numbers of the valleys shown in Fig. 11(d) is derived as  $29610 = \text{floor}(10 \text{ MHz}/405.2592 \text{ kHz} + 1/2) + 29585$ . Finally, the transfer delay of the 500-m fiber can be calculated as  $2451.581661 \text{ ns}$ , which agrees well with the measured delay of  $2451.6 \text{ ns}$  by using the delay measurement application of VNA. This result shows that the measurement range of the proposed system reaches at least 500 m.

#### IV. CONCLUSION

We have demonstrated a novel method for the OFTD measurement, which features high stability and high accuracy simultaneously. A system stability of  $\pm 0.02 \text{ ps}$  and an accuracy of  $\pm 0.07 \text{ ps}$  were achieved in the experiment. A 500-m fiber was also successfully measured, which proves that a measurement range of at least 500 m can be obtained. Benefitting from the high stability, high accuracy, and simple structure, the beam sidelobe suppression ratio of optical phased array antenna systems and the positioning accuracy of 5G systems can be improved. We believe the proposed method may find applications in fiber-optic sensors, optical phased array antenna systems, and large-capacity optical fiber communications. In addition, if polarization-management technology is applied to the measurement path, the proposed system can be implemented using integrated photonics, which will bring a wider range of applications.

#### REFERENCES

[1] J. Capmany and D. Novak, "Microwave photonics combines two worlds," *Nat. Photonics.*, vol. 1, no. 6, pp. 319-330, 2007.

[2] A. Kersey and B. Culshaw, "Fiber-Optic Sensing: A Historical Perspective," *J. Lightwave Technol.*, vol. 26, no. 9, pp. 1064-1078, 2008.

[3] S. Pan and Y. Zhang, "Microwave Photonic Radars," *J. Lightwave Technol.*, doi: 10.1109/JLT.2020.2993166.

[4] W. Yuan, B. Pang, J. Bo and X. Qian, "Fiber Optic Line-Based Sensor Employing Time Delay Estimation for Disturbance Detection and Location," *J. Lightwave Technol.*, vol. 32, no. 5, pp. 1032-1037, 2014.

[5] D. Zhu and S. Pan, "Broadband Cognitive Radio Enabled by Photonics," *J. Lightwave Technol.*, vol. 38, no. 12, pp. 3076-3088, 2020.

[6] F. Zhang, Q. Guo, Z. Wang, P. Zhou, G. Zhang, J. Sun, et al., "Photonics-based broadband radar for high-resolution and real-time inverse synthetic aperture imaging," *Opt. Express*, vol. 25, no. 14, pp. 16274-16281, 2017.

[7] X. Jiang, X. C. Wang, A. R. Zhao, J. P. Yao, and S. L. Pan, "A Multi-Antenna GNSS-over-fiber System for High Accuracy 3D Baseline Measurement," *J. Lightwave Technol.*, vol. 37, no.17, pp. 4201-4209, 2019.

[8] D. Dolfi, F. Michel-Gabriel, S. Bann, and J. P. Huignard, "Two-dimensional optical architecture for time-delay beam forming in a phased-array antenna," *Opt. Lett.*, vol. 16, no. 4, pp. 255-257, 1991.

[9] B. Vidal, T. Mengual, C. Ibanez-Lopez, and J. Marti, "Optical Beamforming Network Based on Fiber-Optical Delay Lines and Spatial Light Modulators for Large Antenna Arrays," *IEEE Photon. Technol. Lett.*, vol. 18, no. 24, pp. 2590-2592, 2006.

[10] B. Wang, C. Gao, W. L. Chen, J. Miao, X. Zhu, Y. Bai, et al., "Precise and Continuous Time and Frequency Synchronisation at the  $5 \times 10^{-19}$  Accuracy Level," *Sci. Rep.*, vol. 2, p. 556, 2012.

[11] B. Lee, "Review of the present status of optical fiber sensors," *Opt. Fiber Technol.*, vol. 9, no. 2, pp. 57-79, 2003.

[12] X. Wang, S. Li, X. Jiang, J. Hu, M. Xue, S. Xu, et al., "High-accuracy optical time delay measurement in fiber link [Invited]," *Chin. Opt. Lett.*, vol. 17, no. 6, p. 060601, 2019.

[13] A. H. Hartog, M. P. Gold, and A. P. Leach, "Optical time-domain reflectometry," *Appl. Opt.*, vol. 16, no. 9, pp. 2375-2379, 1977.

[14] A. Wang and Y. Wang, "Chaos correlation optical time domain reflectometry," *Sci. China Ser. F-Inf. Sci.*, vol. 53, no. 2, pp. 398-404, 2010.

[15] Z. Xie, L. Xia, Y. Wang, et al., "Fiber fault detection with high accuracy using chaotic signal from an SOA ring reflectometry," *IEEE Photon. Technol. Lett.*, vol. 25, no. 8, pp. 709-712, 2013.

[16] W. Eickhoff and R. Ulrich, "Optical frequency domain reflectometry in single-mode fiber," *Appl. Phys. Lett.*, vol. 39, no. 9, pp. 693-695, 1981.

[17] Y. L. Hu, L. Zhan, Z. X. Zhang, S. Y. Luo, and Y. X. Xia, "High-resolution measurement of fiber length by using a mode-locked fiber laser configuration," *Opt. Lett.*, vol. 32, no. 12, pp. 1605-1607, 2007.

[18] K. Yun, J. Li, G. Zhang, L. Chen, W. Yang, and Z. Zhang, "Simple and highly accurate technique for time delay measurement in optical fibers by free-running laser configuration," *Opt. Lett.*, vol. 33, no. 15, pp. 1732-1734, 2008.

[19] J. Dong, B. Wang, C. Gao, Y. Guo, and L. Wang, "Highly accurate fiber transfer delay measurement with large dynamic range," *Opt. Express*, vol. 24, no. 2, pp. 1368-1375, 2016.

[20] S. Li, X. Wang, T. Qing et al., "Optical Fiber Transfer Delay Measurement Based on Phase-Derived Ranging," *IEEE Photon. Technol. Lett.*, vol. 31, no. 16, pp. 1351-1354, 2019.

[21] S. P. Li, T. Qing, J. B. Fu, X. C. Wang, S. L. Pan, "High-Accuracy and Fast Measurement of Optical Transfer Delay," *IEEE Trans. Instrum. Meas.*, accepted July 13, 2020, doi: 10.1109/TIM.2020.3011585.

[22] H. Fu, D. Chen, Z. Cai, "Fiber Sensor Systems Based on Fiber Laser and Microwave Photonic Technologies," *Sensors*, vol. 12, no. 5, pp. 5395-5419, 2012.

[23] L. J. Mullen, V. M. Contarino, P. R. Herczfeld, "Hybrid lidar-radar for medical diagnostics," U.S. Patent 7010339B2, Mar. 7, 2006.

**Shupeng Li** received the B.S. degree from the Nanjing University of Aeronautics and Astronautics, Nanjing, China, in 2015. He is currently working toward the Ph.D. degree at the Key Laboratory of Radar Imaging and Microwave Photonics, Ministry of Education, Nanjing University of Aeronautics and Astronautics. His research interest is in microwave photonics measurement.

**Ting Qing** received the B.S. degree from the Nanjing University of Aeronautics and Astronautics, Nanjing, China, in 2014. She is currently working toward the Ph.D. degree at the Key Laboratory of Radar Imaging and Microwave Photonics, Ministry of Education, Nanjing University of Aeronautics and Astronautics. Her research interest is in microwave photonics measurement.

**Jianbin Fu** received the B.S. degree from the Nanjing University of Aeronautics and Astronautics, Nanjing, China, in 2011. He is currently working toward the Ph.D. degree at the Key Laboratory of Radar Imaging and Microwave Photonics, Ministry of Education, Nanjing University of Aeronautics and Astronautics. He is also with the Suzhou LiuYaoSi Information Technologies Co., Ltd, Suzhou, 215500, China. His research interest is in microwave photonics measurement.

**Xiangchuan Wang** received the B.Eng. degree in automation and the Ph.D. degree in microelectronics and solid-state electronics from Nanjing University, Nanjing, China, in 2009 and 2015, respectively. He is currently an associate professor with the Key Laboratory of Radar Imaging and Microwave Photonics, Ministry of Education, Nanjing University of Aeronautics and Astronautics, Nanjing, China. His current research interests include microwave photonic measurement and optical fiber sensing technologies.

**Shilong Pan** (S'06–M'09–SM'13) received the B.S. and Ph.D. degrees in electronics engineering from Tsinghua University, Beijing, China, in 2004 and 2008, respectively. From 2008 to 2010, he was a “Vision 2010” Postdoctoral Research Fellow with the Microwave Photonics Research Laboratory, University of Ottawa, Canada. He joined the College of Electronic and Information Engineering, Nanjing University of Aeronautics and Astronautics, China, in 2010, where he is currently a Full Professor and an Executive Director with the Key Laboratory of Radar Imaging and Microwave Photonics, the Ministry of Education.